

Geophysical Research Letters*



RESEARCH LETTER

10.1029/2023GL102763

Key Points:

- The 15 January 2022 Hunga Tonga-Hunga Ha'apai eruption had four episodic seismic subevents with similar waveforms within ~300 s
- An unusual upward force jump-started each subevent
- A magma hammer explains the force and estimates the subsurface magma mass flux which fits the vent discharge rate based on satellite data

Supporting Information:

Supporting Information may be found in the online version of this article.

Correspondence to:

Y. Zheng, yzheng12@uh.edu

Citation:

Zheng, Y., Hu, H., Spera, F. J., Scruggs, M., Thompson, G., Jin, Y., et al. (2023). Episodic magma hammers for the 15 January 2022 cataclysmic eruption of Hunga Tonga-Hunga Ha'apai. *Geophysical Research Letters*, 50, e2023GL102763. https://doi.org/10.1029/2023GL102763

Received 4 JAN 2023 Accepted 30 MAR 2023

Author Contributions:

Conceptualization: Yingcai Zheng, Frank J. Spera, Melissa Scruggs, Yuesu Jin, Tom Lapen, Stephen R. McNutt, Dave A. Yuen

Data curation: Hao Hu, Glenn Thompson

Formal analysis: Yingcai Zheng, Hao Hu, Frank J. Spera, Melissa Scruggs, Glenn Thompson, Yuesu Jin, Tom Lapen, Stephen R. McNutt, Kyle Mandli, Zhigang Peng, Dave A. Yuen Investigation: Yingcai Zheng, Hao Hu, Frank J. Spera, Melissa Scruggs, Glenn Thompson, Yuesu Jin, Tom Lapen, Stephen R. McNutt, Kyle Mandli, Zhigang Peng, Dave A. Yuen

© 2023. The Authors.

This is an open access article under the terms of the Creative Commons Attribution License, which permits use, distribution and reproduction in any medium, provided the original work is properly cited.

Episodic Magma Hammers for the 15 January 2022 Cataclysmic Eruption of Hunga Tonga-Hunga Ha'apai

Yingcai Zheng¹, Hao Hu¹, Frank J. Spera², Melissa Scruggs², Glenn Thompson³, Yuesu Jin¹, Tom Lapen¹, Stephen R. McNutt³, Kyle Mandli⁴, Zhigang Peng⁵, and Dave A. Yuen⁴

¹Department of Earth and Atmospheric Sciences, University of Houston, Houston, TX, USA, ²Department of Earth Science, University of California, Santa Barbara, Santa Barbara, CA, USA, ³School of Geosciences, University of South Florida, Tampa, FL, USA, ⁴Department of Applied Physics and Applied Mathematics, Columbia University, New York, NY, USA, ⁵School of Earth and Atmospheric Sciences, Georgia Institute of Technology, Atlanta, GA, USA

Abstract Understanding the forces and magma system dynamics on timescales of seconds to minutes remains challenging. In the January 2022 phreatoplinian Hunga Tonga-Hunga Ha'apai eruption, four remarkably similar seismic subevents within a 5-min interval occurred during the intensifying early eruptive phase. The subevents are similar in waveforms and durations (~25 s each). Each subevent begins with an unusual negative P-wave polarity which is inferred, using full-wave seismic modeling, to be caused by an upward single-force mechanism at the volcano created by a magma hammer likely in response to magma flow blockage/constriction during the early part of the eruption as discharge rapidly increased over orders of magnitude with concomitant conduit geometry evolution and instability. Our proposed episodic magma hammer model is consistent with thermodynamic and phase properties of the magmatic mixture, and yields an estimate of conduit mass flow in agreement with vent discharge rates derived from satellite imagery of plume heights.

Plain Language Summary The seismic record of the 15 January 2022 Hunga Tonga-Hunga Ha'apai explosive eruption exhibited a remarkably regular pattern, recording repeating volcanic processes. Within an interval of ~300 s during an early eruptive phase, four strong seismic subevents occurred and were recorded by global seismic stations. Detailed seismic analyses showed that each of these subevents is similar in waveform and duration and is characterized by a sequence of four forces: upward, downward, upward, and downward. We suggest that the first upward seismic force at the volcano was likely created by an ascending magma colliding with a blockage or conduit constriction that occurred during and because of the ongoing eruption. We attribute the other forces to upward magma backflow and piston motion in the conduit, owing to their similar time durations. The magma hammer mechanism allows us to estimate the magma flow rate in the subsurface conduit, which is consistent with the vent discharge rate observed by satellite imagery.

1. Introduction

The Hunga Tonga-Hunga Ha'apai (HTHH) volcano erupted violently on 15 January 2022 generating a spectacular ensemble of planetary-scale signals (Matoza et al., 2022; Terry et al., 2022; Wright et al., 2022; Xu et al., 2022; Yuen et al., 2022), including: audible sounds heard in New Zealand and Alaska, the tallest recorded volcanic plume (peak height ~ 58 km), >400,000 lighting flashes, a locally destructive tsunami wave (Borrero et al., 2022), a global meteotsunami traveling at the speed of sound (Carvajal et al., 2022; Imamura et al., 2022; Kubota et al., 2022), and infrasound and seismic waves that circled the Earth multiple times (Amores et al., 2022; Vergoz et al., 2022). In this study, we focus on the unusual repeating subsurface episodic seismic signals during the early intensifying phase of the eruption.

1.1. Geological Background

HTHH is one of many island-arc volcanoes formed because of fast (200–250 mm/year) subduction of the Pacific Plate beneath the Indo-Australian plate along the Tonga-Kermadec arc (Smith & Price, 2006; Wei et al., 2016). For HTHH magmas, juvenile $\rm H_2O$ concentrations are ~4–5 wt%, reaching saturation at 5–7 km depths (Brenna et al., 2022) (see also Text S2 in Supporting Information S1). Crystallization and the concomitant increase in volatile concentrations lead to the development of magma overpressure and the consequent propagation of

ZHENG ET AL. 1 of 13

9448007, 2023, 8, Downloaded from https://agupubs.onlinelibrary.wiley

.com/doi/10.1029/2023GL102763, Wiley Online Library on [03/09/2023]. See the Terms and Conditions (https://onlinelibrary.wiley.com/terms-

and-conditions) on Wiley Online Library for rules of use; OA articles are governed by the applicable Creative Commons License

magma-filled fractures to the surface (Brenna et al., 2022; Fowler & Spera, 2008; Lister & Kerr, 1991; Tait et al., 1989).

1.2. Timings of Various Volcanic Phenomena

Historically, HTHH is a large submarine edifice that has experienced small-scale submarine and Surtseyan activity (Cronin et al., 2017; GVP, 1988, 2009a, 2009b, 2015, 2022a) between large, caldera-forming eruptions (Brenna et al., 2022) (see Figure 1). The latest period of activity began on 20 December 2021, ultimately culminating in the cataclysmic 15 January 2022 eruption (Figure 1b). An eruption on 13 January at 15:20 UTC (04:20 14 January local time) produced a 20 cm tsunami and a 20 km tall plume, accompanied by ~190,000 lightning flashes (GVP, 2022b)—and even partially destroyed a land mass formed during the 2014–2015 eruption that connected the islands of Hunga Tonga and Hunga Ha'apai (Cronin et al., 2017). An overnight eruption totally removed this land mass in the early morning hours of 15 January, before the final, most intense eruptive phase began.

The 15 January volcanic eruption did not begin abruptly. Instead, an ensemble of time-transgressive phenomena overlapped (Figure 1c). The USGS reported a M5.8 seismic event with an origin time of 04:14:45 15 January 2022 (UTC), located at 20.546°S, 175.390°E with 0 km depth. This time cannot be the start time of the eruption, as satellite imagery captured at 04:10 UTC shows a rapidly growing volcanic plume already 18 km high—eventually peaking at mesospheric heights of ~58 km around 04:30 UTC (Yuen et al., 2022). Extrapolating the infrasound signals in time and distance back to the volcanic location gives an eruption inception time around 04:02 ± 1 UTC (Yuen et al., 2022), which is more consistent with observed plume heights and the recent IMS infrasound analysis (Vergoz et al., 2022). Residents of nearby islands reported ashfall persisting throughout the night, suggesting an eruption duration of ~12 hr (Yuen et al., 2022). Although the precise timing of the symphony of phenomena remains uncertain, an uptick in lightning intensity around 04:12 UTC is consistent with a strong eruptive pulse starting at 04:07–04:09 UTC (Figure 1c), allowing for an estimated 5-min delay between plume ascent and lightning onset, consistent with previous studies of volcanic lightning (Behnke et al., 2013; Hoblitt, 1994). The rapid increase in lightning after 04:12 UTC is consistent with high mass flow at the vent around 04:08 UTC. These phenomena indicate that the eruption was well underway before the 04:15 UTC seismic event analyzed in detail below.

2. Data and Results

Our seismic analysis involves minimal processing of the raw records. We first downloaded seismic waveforms recorded worldwide from Incorporated Research Institutions for Seismology (IRIS), removed their instrumental responses, and high-pass filtered traces with a corner frequency 0.01 Hz. Theoretical travel times of the direct P waves for all the stations using the USGS reported origin time and location and a crosscorrelation were used to align the waveforms (Figure 2b) (Yu et al., 2017). We selected 417 stations (Figure 2a) based on the signal-noise-ratio (SNR > 1.6) defined as the ratio of the root-mean-squares amplitude in the P-wave signal window (within 60 s following the P time) and the noise window (within 60 s before the P time). Shifted waveforms were stacked to obtain the seismic wavelet used to study the source process (Figure 3).

2.1. Unusual Repeating Episodic Seismic Signals Recorded Worldwide

Within a time of \sim 300 s immediately after the reported seismic event, four subevents—E-1, E-2, E-3, and E-4—are visible in both the stacked ground displacement and velocity seismograms (Figures 3a and 3b). Each subevent has a similar duration of \sim 25 s. If these were regular tectonic earthquakes, a 25 s source duration would result in an event of around Mw7.5, far greater than the reported magnitude M5.8 by USGS. A 204.6 s time interval occurs between subevents E-1 and E-2, \sim 39.8 s between E-2 and E-3, and \sim 25.4 s between E-3 and E-4; note that the tail end of E-3 overlaps the beginning part of subevent E-4 (Figure 3). Each subevent can be further divided into four consecutive eruption stages A/B/C/D (Figures 3c–3e) with respective durations 3 s/15 s/3 s/3 s. We call the subevents E-1 to E-4 "episodic" because they have similar waveforms (Figures 3c–3e; Figures S1 and S2 in Supporting Information S1), indicating that similar eruption dynamics likely governed these subevents.

2.2. Source Mechanism

First, polarities of the farfield *P*-wave first motions for the subevents (E1, E2, and E3) are found to be downward (dilatational) in the globally and azimuthally stacked (Figure 3 Stage-A's; Figure S1 in Supporting

ZHENG ET AL. 2 of 13



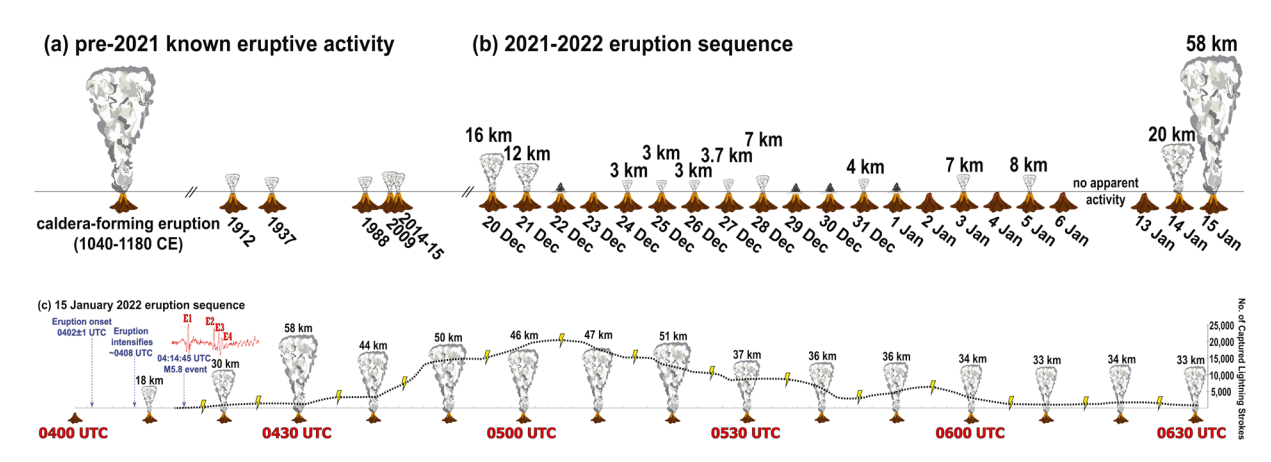


Figure 1. Timeline of events leading up to and including the onset of the 15 January 2022 eruption of Hunga Tonga-Hunga Ha'apai (HTHH). Eruption column heights (labeled by numbers) and eruptive history are reported by the Global Volcanism Program (GVP, 1988, 2009a, 2009b, 2015, 2022a, 2022b) and by our analysis of available satellite imagery (e.g., Yuen et al., 2022). For days where no eruptive activity was noted, volcano symbols show no eruption. Days with eruptive activity but no substantial eruption column are marked by lava on the volcano symbols with Surtseyan eruptions, and eruption columns are to-scale for those days where substantial plume development was reported. Volcanic lightning data are also shown in black dashed line with lightning icons (Yuen et al., 2022).

Information S1). Secondly, the azimuthally stacked P waveforms are highly similar which shows the radiated P-wave is mostly azimuthally symmetric (Figure S2 in Supporting Information S1). Thirdly, this symmetry property is further supported by a lack of visible energy in the transverse component in the stacked S waves (see Figure S2 in Supporting Information S1). These characteristics suggest that the subevents were not caused by earthquake dislocation faulting or landslides on the volcano flank, but rather by forces with mostly azimuthal symmetry to the first order.

An azimuthally symmetric source consistent with negative polarity could be: a single force in the vertical direction, or an implosion, or a CLVD source (Knopoff & Randall, 1970) at the volcano. Using the stacked wavelet as the source time function (Figure 3a), our detailed full-wave seismic modeling (see Text S1 in Supporting Information S1) showed single forces in the vertical direction are preferred over either implosion or CLVD because (a) the synthetic waveforms can fit the observed data for both body waves (Figure S3 in Supporting Information S1) and surface waves (Figure S4 in Supporting Information S1) in both vertical and radial components; (b) waveform synthetics due to an implosion/explosion or a CLVD source show strong P-to-S converted waves at \sim 600 s, which are not observed in the seismic records (see Figures S5 and S7 in Supporting Information S1), despite the fact that they can fit the surface waves well (Figures S6 and S8 in Supporting Information S1).

We also investigated if the single forces were truly vertical by examining the subtle azimuthal variations in the locally averaged P-wave amplitudes of E1, E2, and E3 (Figure S9 in Supporting Information S1). Similarities in the azimuthal trends of E1, E2, and E3 amplitudes strongly suggest that the four subevents have an identical or closely related physical origin. We find that a tilted force fits the observed azimuthal P-amplitudes better (Figure S9 in Supporting Information S1). The tilted single force is along the line containing the vector [1, 0.08, 0.46] in [Upward, North, West] directions, respectively. This force has a ~25.0-degree tilt with respect to the true vertical direction. Furthermore, regional surface wave modeling using this tilted single-force and stacked source wavelets (Figure 3) provided a satisfactory match between modeled and observed waveforms in all three components (Figure S10 in Supporting Information S1). Note that we used the 1-dimensional PREM (Dziewonski & Anderson, 1981) model in the full waveform modeling (not taking into account the heterogenies in the Earth) so perfect matching between the data and the modeled waveforms is not expected. The explosion mechanism explored by Thurin et al. (2022) is not consistent with data in two aspects: the negative P-wave first motion polarity and the above-mentioned converted S waves in the modeled waveforms ~600 s. Thurin et al. (2022) were not able to model multicomponent regional surface waves and body waves using single forces whereas we are able to fit both types of multicomponent data. Their poor waveform fitting could be caused by their use of Gaussian wavelets which have only one polarity. However, it is evident that the stacked source wavelets are not Gaussian (Figure 3). Poli and Shapiro (2022) used single force to estimate the Volcanic Explosivity Index. Garza-Girón et al. (2022) set the single-force history to be downward a priori and they considered our E2 \sim E4 not as independent episodic events. We are not to say that during the \sim 12 hr HTHH eruption explosions did not take place, but only that for the records studied here, explosions can be excluded.

ZHENG ET AL. 3 of 13

1944807, 2023, 8, Downloaded from https://agupubs.onlinelibrary.wiley.com/doi/10.1029/2023GL102763, Wiley Online Library on [03/09/2023]. See the Terms and Conditions (https://onlinelibrary.wiley.com/terms-and-conditions) on Wiley Online Library for rules of use; OA articles are governed by the applicable Creative and Conditions (https://onlinelibrary.wiley.com/terms-and-conditions) on Wiley Online Library for rules of use; OA articles are governed by the applicable Creative and Conditions (https://onlinelibrary.wiley.com/terms-and-conditions) on Wiley Online Library for rules of use; OA articles are governed by the applicable Creative and Conditions (https://onlinelibrary.wiley.com/terms-and-conditions) on Wiley Online Library for rules of use; OA articles are governed by the applicable Creative and Conditions (https://onlinelibrary.wiley.com/terms-and-conditions) on Wiley Online Library for rules of use; OA articles are governed by the applicable Creative and Conditions (https://onlinelibrary.wiley.com/terms-and-conditions) on Wiley Online Library for rules of use; OA articles are governed by the applicable Creative and Conditions (https://onlinelibrary.wiley.com/terms-and-conditions) on Wiley Online Library for rules of use; OA articles are governed by the applicable Creative and Conditions (https://onlinelibrary.wiley.com/terms-and-conditions) on Wiley Online Library for rules of use; OA articles are governed by the applicable Creative and Conditions (https://onlinelibrary.wiley.com/terms-and-conditions).

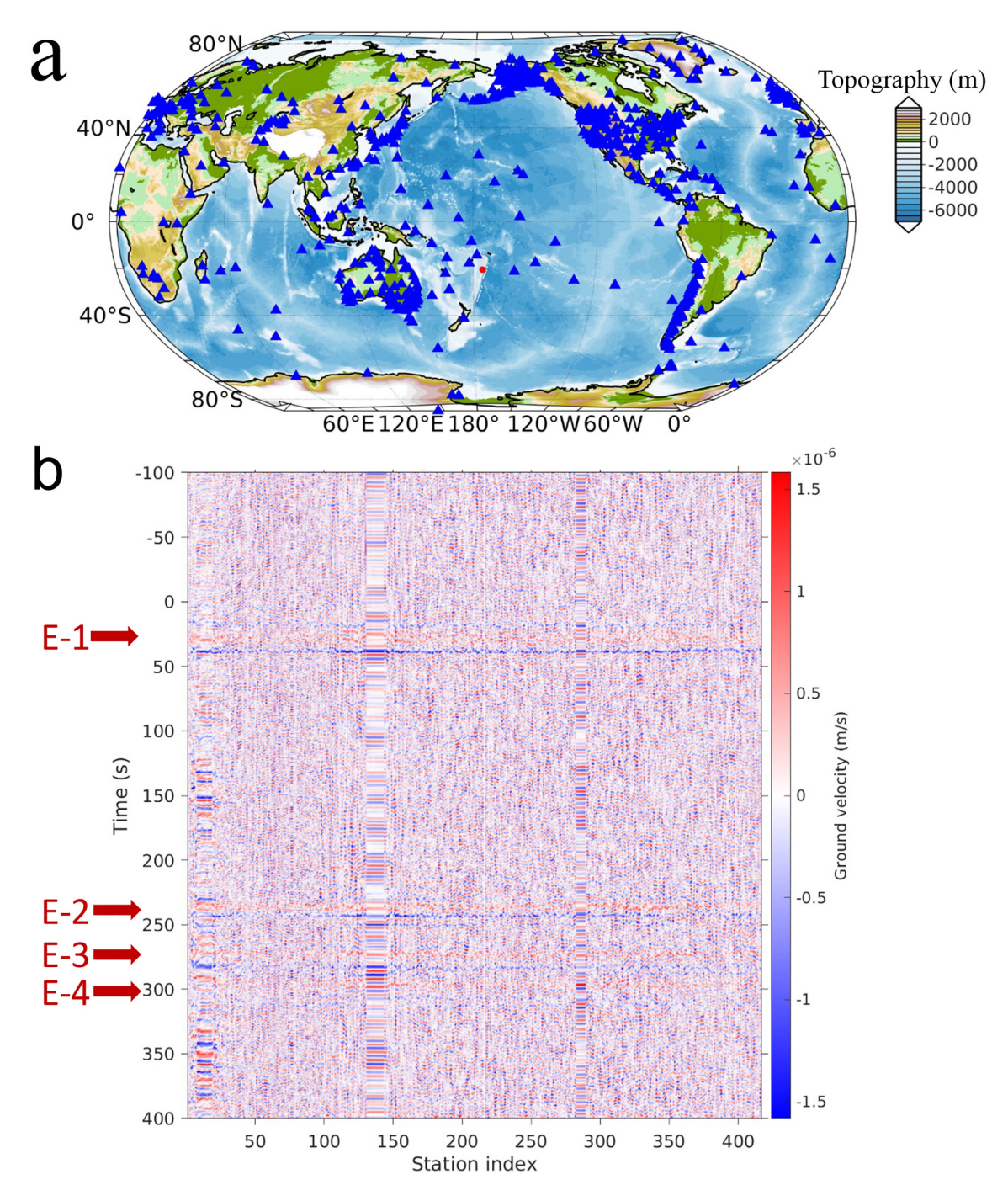


Figure 2. Global seismic signals. (a) Distribution of global seismometers (blue triangles) used in this study and the Hunga Tonga-Hunga Ha'apai volcano (red dot); (b) Aligned seismograms based on the picked direct P-wave travel times showing four global subevents. The seismograms are vertical-component ground velocities, high-pass filtered with a corner frequency of 0.01 Hz. The stations are aligned by the epicentral distance.

3. Eruption Stages and the Magma Hammer Mechanism

As the lack of subsurface information precludes obtaining well-constrained parameters for any HTHH dynamic model, the purpose of our simplified analysis is to present a mechanism which aligns with the unusual observed seismicity of the 15 January eruption and the calculated forces involved, while also agreeing with the observed development of the eruption plume and magma properties.

ZHENG ET AL. 4 of 13

1944807, 2023, 8, Downloaded from https://agupubs.onlinelibrary.wiley.com/doi/10.1029/2023GL102763, Wiley Online Library on [03:09/2023]. See the Terms and Conditions (https://onlinelibrary.wiley.com/terms-and-conditions) on Wiley Online Library for rules of use; OA articles are governed by the applicable Creative Commons Licensea

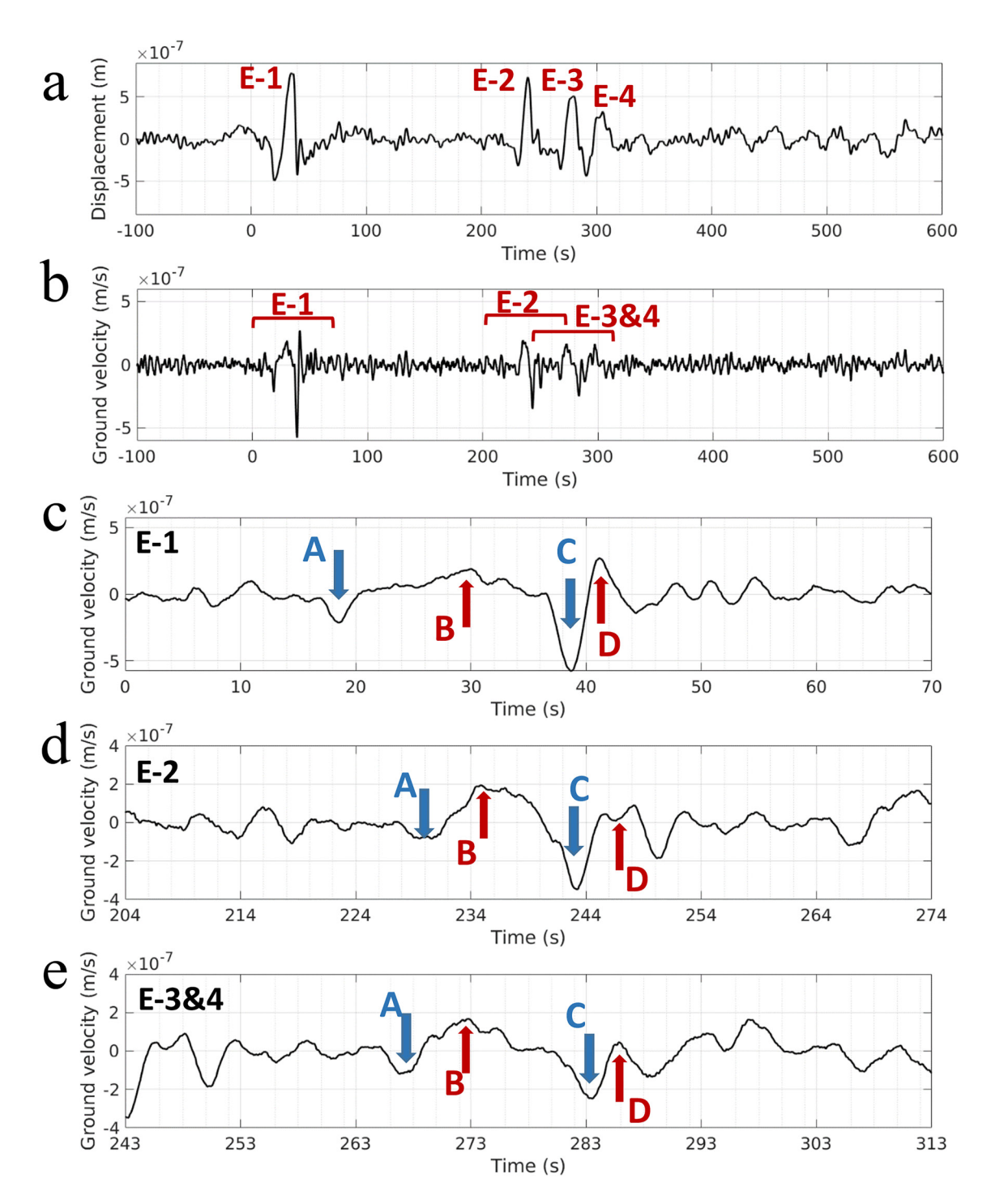


Figure 3. Source wavelet produced by stacking globally recorded seismic signals. The vertical-component seismograms are highpass filtered above a corner frequency 0.01 Hz; (a) stacked ground displacement showing four sub-eruptions, E-1–E-4; (b) stacked ground velocity seismogram showing E1~E4. Zoomed-in velocity seismograms are shown around (c) uE-1, (d) E-2, and (e) E-3 and E-4. Stages for E-4 are not labeled because E-4 and E-3 have overlap. Time zero corresponds to the USGS reported seismic event origin time 04:14:45 15 January 2022 (USGS, 2022). However, E1A begins at about 04:15:00.

Based on the stacked P-wave seismograms (Figures 3b–3e), we attempt to decipher the four eruptive stages (A, B, C and D) in the context of conduit flow through magma-conducting conduits for each of the subevents. Because each of the seismic subevents exhibits similar waveforms, we focus our analysis on the E-1 subevent time series (Figure 4). The respective durations for Stages A to D are \sim 3 s, 15 s, 3 s, and 3 s, with correlating the single-force directions of up/down/up/down, respectively (Figure 4b). Volcanic seismic sources usually give rise

ZHENG ET AL. 5 of 13

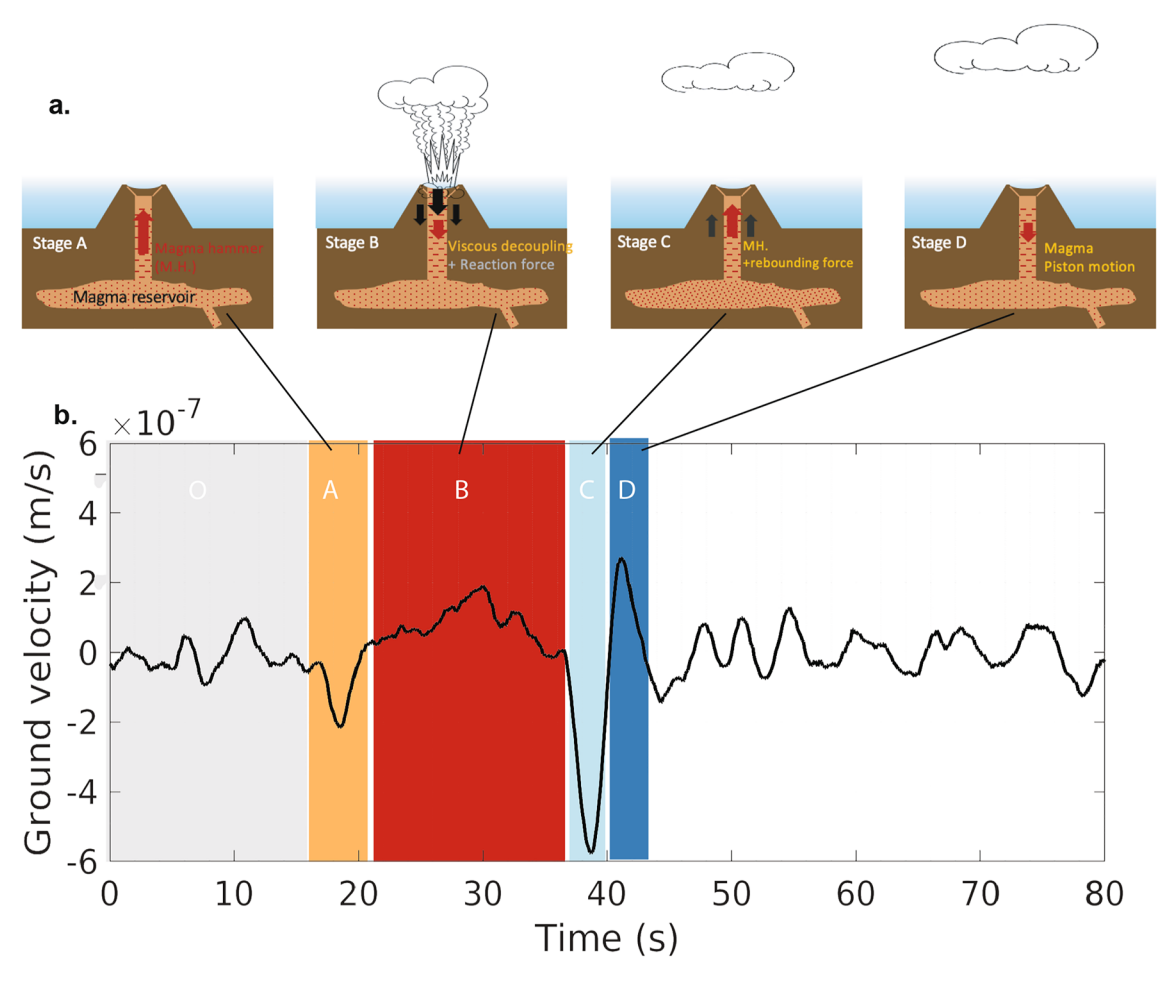


Figure 4. Eruption stages and magma plumbing system. (a) Volcano-reservoir schematics of states and forces (red arrow: magma hammer; black arrow: reaction force) corresponding to Stages A–D. The magma reservoir is centered at depth of 5–8 km based on geobarometry (Brenna et al., 2022). (b) Globally stacked ground velocity (vertical component) of event E-1. The amplitude of the waveform is not linearly proportional to the force history (Figure S11b in Supporting Information S1). Time zero corresponds to ~04:14:45 15 January 2022.

to a combination of moment-tensor force couples and single-forces (B. A. Chouet & Matoza, 2013). Single-forces in the up-down direction rather than resolved force-couples are rare. In this regard, this HTHH eruption shares some striking similarities to the 2004 Mt. Asama activity (the most active volcano in Honshu Japan), which has well-resolved down/up/down single-forces in three stages for five episodic similar events that occurred over a ~2.5 month period (Ohminato et al., 2006). Like HTHH, Mt. Asama also generated a strong air shock (Ohminato et al., 2006) indicative of a strong under-expanded volcanic jet with a vent magma pressure exceeding ambient atmospheric pressure. In the following, we use well-established ideas to discuss the four stages A~D we have found. Although there is no doubt phreatomagmatic activity can play a role in generating local and regional seismic signals, its role on teleseismic signal generation is probably not very significant for the following two reasons. First, the earlier Jan 14 HTHH eruption generated no coherent global teleseismic signals, although strong phreatomagmatic activities and explosions occurred. Second, the 2004 eruption of Mt. Asama involved neither phreatic nor phreatomagmatic activity (GVP, 2004).

Mechanisms for producing upward forces include: viscous drag force along the conduit wall due to a steady state upward magma motion (Coppess et al., 2022; Ohminato et al., 2006), magma return flow at some barrier due to a uprising gas plug push (B. Chouet et al., 2003) (similar to the water-hammer effect), and constriction of flow (Morrissey & Chouet, 1997) akin to hydraulic shock (Kieffer, 1984; Morrissey & Chouet, 1997; St. Lawrence & Qamar, 1979; Streeter & Wylie, 1974; Yin, 2018). In the conventional 1-D water-hammer mechanism, water flows steadily through a pipe with an open valve. Rapid closure of this valve creates a surge of water hammer pressure P_H , acting on the closure point which can sometimes burst a steel pipe. The effect can also

ZHENG ET AL. 6 of 13

be due to a piston of fluid impacting on an obstructive barrier (B. Chouet et al., 2003) such as a volcanic plug (Iverson et al., 2006) or flowing through a constriction (Morrissey & Chouet, 1997). We do not know whether such elements exist or not in the HTHH subsurface. However, our rudimentary magma-hammer model yields a remarkably consistent estimate of magma flux comparable to the vent discharge rate. Here, we sketch the basic water-hammer concept (necessarily simplified due to lack of subsurface information), modified to the parameters of a multi-phase magma.

Mathematically, the water-hammer pressure, P_H , can be described by the well-known Joukowsky equation (Streeter & Wylie, 1974) for slow fluid flow (V << c): $P_H = \rho c V$, where ρ is the fluid density, c is the sound speed in the fluid, and V is the fluid flow speed in the pipe. Since magma is involved here rather than water, we apply the term *magma hammer* to describe this process.

4. Discussion of Forces in the Eruption Stages

Before Stage-A (time <15 s in the record), the stacked seismic record is characterized by fluctuating ground motion (Figure 4b). Based on infrasound wave speeds and satellite imagery (Yuen et al., 2022) the magma transport conduit had already connected to a surface vent and the plume had likely already been established.

4.1. Stage A: Magma Hammer and Estimates of Magma Flux and Discharge

Stage-A (E-1A) lasted about \sim 3.2 s and the farfield ground motion was characterized by a distinct downward ground motion, meaning that the seismic source was likely to be an upward single-force (Figure S11c in Supporting Information S1). Full-wave seismic modeling (Text S1 in Supporting Information S1) reveals that this upward single-force source has a force magnitude \sim 5.0 \times 10¹² N (Text S1 in Supporting Information S1; Figure S3–S8). We argue that Stage A of E-1 \sim E-4 with similar ground displacements represents magma hammer breaching of a short-lived flow blockage of the magma conduit such as a caldera plug, generating an upward single force.

4.1.1. Magma Hammer and Piston Motion

Multiplying both sides of the Joukowsky equation $(P_H = \rho cV)$ by the cross-sectional area, A, of the flow conduit, we get $F_H = P_H A = \rho cQ_V = cQ_m$, where the hammer force, F_H , can be directly estimated by the seismic modeling $(\sim 5 \times 10^{12} \ N$ for Stage-A; Figure S11b in Supporting Information S1), $Q_V = VA$ is the magma volume flux (in m³/s), and $Q_m = \rho VA$ is the magma mass flux (in kg/s), in the subsurface plumbing system. It is important to note that in this expression, magma density is that of the magmatic mixture of melt plus fluid (see Texts S2 and S3 in Supporting Information S1 for details).

4.1.2. Magma Equation of State and Flux Estimates

We now consider magma composition, degree of volatile saturation, and flow regime. Equilibrium crystallization of the last-erupted HTHH andesites was modeled using rhyolite-MELTS (Gualda & Ghiorso, 2015) to approximate the state of an andesitic magma as it undergoes closed-system degassing and ascends adiabatically to the surface from a reservoir depth of \sim 7.5 km (P=2 kbar). The state of the magma body was recorded at each P-Talong an isentropic path and the volume fraction of the exsolved volatiles calculated (Text S2 in Supporting Information S1; Figure S12 in Supporting Information S1). The sonic velocity of a two-phase (melt + fluid) mixture was then computed for both bubbly flow (i.e., well mixed) and slug flow (i.e., gas pockets) regimes (see details in Text S3 in Supporting Information S1, Figures S13 and S14 in Supporting Information S1). We argue that slug flow is more likely, given the explosiveness of the eruption and short time scales involved although in a complex volcanic eruption it would seem reasonable to assume that both flow regimes may exist simultaneously at different locations and different times. Taking into account uncertainties, the sound wave speed in magma is estimated to be, $c \sim 1,000-2,000$ m/s, and we can get a mass flux $Q_m \sim 0.5 - 5 \times 10^9$ kg/s using the peak force in E-1A. Approximating the seismic wavelet in E-1A as a triangle, the average force should be halved. Alternatively, we can estimate the volcanic discharge into the atmosphere (Carey & Bursik, 2015). According to satellite images of the volcanic plume heights, the mass flow to support a 58 km volcanic plume from Yuen et al. (2022) is $\sim 1.4 \times 10^9$ kg/s. Our proposed magma-hammer model is consistent to within an order of magnitude or better with the force estimated from the seismic data, estimated vent discharge estimate into the atmosphere, physiochemical magma properties, and sonic velocities.

ZHENG ET AL. 7 of 13

9448007, 2023, 8, Downloaded from https://agupubs.onlinelibrary

com/doi/10.1029/2023GL102763, Wiley Online Library on [03/09/2023]. See the Terms

articles are governed by the applicable Creative Commons Licens-

4.2. Stage B: Eruption of Volcanic Jet

Stage E-1B—a downward single force at the volcano—is the longest stage (15 s) in all four stages (Figure 4a). It is likely due to the reactive impulsive force associated with opening of the magmatic conduit and transient reestablishment of intense outflow for \sim 15 s (Figure 4a). The eruption could have sent a series of pulses of volcanic product (ash, pyroclasts, crystals, lithics and seawater-derived steam) into the atmosphere based on observed maximum plume heights referred to earlier. This "upside-down rocket"-type eruption created a downward single-force on the order of \sim 9 × 10¹² N (Figure S11b in Supporting Information S1). The magnitude of the force is comparable to that of the Mount St. Helens 1980 eruption (Kanamori & Given, 1982) of \sim 10¹³ N. Explosive magma fragmentation, which is a complex process, could decrease the magma viscosity and decouple the upward viscous drag force along the conduit wall to create a downward force (Coppess et al., 2022; Ohminato et al., 2006). In Stage-B, the net force first increases then decreases and both upward force and downward forces may coexist. If this is the case, seismic data and modeling show that the downward forces dominate toward the early part of the stage.

4.3. Stages C and D

Stage E-1C, initiated about 20 s after the onset of E-1A, exhibits an upward force of $\sim 4 \times 10^{12}$ N (Figure S11b in Supporting Information S1), and the downward force in E-1D is $\sim 3 \times 10^{12}$ N. We associate Stage-C with a second-phase closing/constricting of the conduit and the subsequent generation of an upward magma-hammer force or viscous drag upward force (details in Text S3 in Supporting Information S1). Stage E-1B exerted a sustained downward force, probably depressing both the less-fragmented magma in the conduit (Ohminato et al., 2006), the magma chamber and surrounding rock. At the end of E-1B, the force has diminished significantly and the possibility of the conduit elastically shrinking inward rapidly nearest the surface increases. Gravity can also assist this conduit closure as the second-order azimuthal variation in P-wave amplitudes suggests the conduit may be slightly tilted to the west with respect to the vertical (Text S1.3 in Supporting Information S1; Figure S9 in Supporting Information S1). The westward tilt is consistent with the post-eruption earthquake locations (Kintner et al., 2022). It is likely that Stage E-1C is related to the magma backflow impacting the overburden rock containing the constricted conduits, which creates an upward magma-hammer force and an upward viscous drag force due to the flow velocity. E-1D seems to be a reflected magma-hammer signal traveling down, which created a downward force as viscous drag or impact of the magma chamber. Stages E-1C and E-1D represent one cycle of oscillatory piston motion as magma motion travels through the conduit, from the reservoir to the surface. After E-1D (>45 s in Figure S4b in Supporting Information S1), we can see regular oscillating piston motions with a period $T \sim 9$ s (Figure S11b in Supporting Information S1). Taking an estimated average traveling sonic velocity of $c \sim 1,000-2,600$ m/s (Figure S13 in Supporting Information S1), we can determine the depth of the magma chamber at $cT/4 \sim 2.25 - 5.85$ km using the formula given by Kieffer (1984), consistent with the geobarometric estimates (Brenna et al., 2022).

4.4. Episodic Seismic Events

Stages A-D for the E-1 event were repeated at least in E-2 and E-3 and likely also in E-4; E-4 is obfuscated by E-3, hindering our ability to clearly read the entire E-4 record (Figure 3). These large magnitude forces are short in duration and could produce the loud audible sounds as recorded by observers and infrasonic sensors around the world (Yuen et al., 2022). The repeated large magma forces can fracture the caldera basement and ballistically remove fractured rocks to excavate the caldera deeper and deeper, eventually forming a 600 m depression as shown in a recent bathymetry map (Cronin and Tonga Geological Services, 2022). The time intervals between the subevents (\sim 204.6, \sim 39.8, and \sim 25.4 s) are long enough to allow for the conduit to be plugged again for additional magma hammers associated with geometric instabilities within the magma transport system.

The explosive HTHH eruption reveals a rapid but regulated nature of shallow magma transport dynamics manifested as episodic magma hammers. Examination and modeling of the seismic data suggest that HTHH produced the largest known magma-hammer force associated with a violent volcanic eruption. Future work will benefit from new 3D marine seismic imaging of the plumbing system to forecast future catastrophic eruption using the episodic nature of this system.

ZHENG ET AL. 8 of 13

5. Conclusions

The 15-Jan-2022 HTHH eruption produced global seismic wavefields. Four episodic seismic events have been identified within a time window of \sim 300 s in the intensifying phase of the volcanic activity. The four subevents have similar waveforms and durations. A westward tilted single force mechanism can fit well both the teleseismic waveforms and the regional surface waves. The magma hammer is one possible mechanism to cause the single force. The magma hammer also provides a way to estimate the conduit magma mass flux which is consistent with the vent discharge estimated from satellite imagery and magma properties.

Conflict of Interest

The authors declare no conflicts of interest relevant to this study.

Data Availability Statement

Thermodynamic properties and phase relations of magma and volatiles at different temperatures and temperatures are given in the Excel file deposited in the Texas Data Repository https://doi.org/10.18738/T8/W6JN20 (last accessed 11 April 2023). The facilities of IRIS Data Services, and specifically the IRIS Data Management Center (https://ds.iris.edu/ds/nodes/dmc/, last accessed 27 December 2022), were used for access to seismic waveforms and related metadata used in this study. IRIS Data Services are funded through the Seismological Facilities for the Advancement of Geoscience (SAGE) Award of the National Science Foundation under Cooperative Support Agreement EAR-1851048. We downloaded data from network codes 2O, AK, AT, AU, AV, AZ, BK, C, C0, C1, CC, CH, CI, CM, CN, CU, CZ, DK, EI, G, GB, GE, GR, GS, GT, HV, IC, II, IM, IU, IW, JP, LD, LX, MN, MX, NA, N4, NL, NM, NU, NZ, OE, PL, PM, PS, PY, RO, SB, SC, SG, SS, TA, TX, UO, US, UU, WM, and WY. A full citation list of the networks accessed and used in this study is in References section (Alaska Earthquake Center, Univ. of Alaska Fairbanks, 1987; Alaska Volcano Observatory/USGS, 1988; Albuquerque Seismological Laboratory (ASL)/USGS, 1980, 1988, 1990, 1992, 1993, 2003, 2006, 2013; Bureau of Economic Geology and The University of Texas at Austin, 2016; California Institute of Technology and United States Geological Survey Pasadena, 1926; Cascades Volcano Observatory/USGS, 2001; Charles University in Prague (Czech) et al., 1973; Colorado Geological Survey, 2016; Dublin Institute for Advanced Studies, 1993; Federal Institute for Geosciences and Natural Resources, 1976; GEOFON Data Centre, 1993; Glanville, 2019; GNS Science, 2021; Incorporated Research Institutions For Seismology, 1970; INGEOMINAS - Servicio Geologico Colombiano (SGC Colombia), 1993; Institut de physique du globe de Paris (IPGP) and École et Observatoire des Sciences de la Terre de Strasbourg (EOST), 1982; Instituto Dom Luiz (IDL) - Faculdade de Ciências da Universidade de Lisboa, 2003; Instituto Nicaraguense de Estudios Territoriales (INETER), 1975; Instituto Português do Mar e da Atmosfera, I.P., 2006; IRIS Transportable Array, 2003; KNMI, 1993, 2006; Lamont Doherty Earth Observatory (LDEO), Columbia University, 1970; MedNet Project Partner Institutions, 1990; Multiple Operators, 1997; National Institute for Earth Physics (NIEP Romania), 1994; Natural Resources Canada (NRCAN Canada), 1975; NOAA National Oceanic and Atmospheric Administration (USA), 1967; Northern California Earthquake Data Center, 2014; Red Sísmica Mexicana, n.d.; San Fernando Royal Naval Observatory (ROA) et al., 1996; Scripps Institution of Oceanography, 1986; Swiss Seismological Service (SED) At ETH Zurich, 1983; UC San Diego, 1982; UC San Diego, 2014; UC Santa Barbara, 1989; Universidad de Chile, 2012; University of Oregon, 1990; University of Utah, 1962, 1983; USGS Hawaiian Volcano Observatory (HVO), 1956; ZAMG – Zentralanstalt für Meterologie und Geodynamik, 1987).

Acknowledgments

We acknowledge the support by the following funding sources: NSF EAR-2027150 (Y. Zheng), EAR-2151039 (FJS), EAR-1918126 (DA Yuen), and DOE DE-SC0019759. We also thank Prof. Victor Tsai and another anonymous reviewer to review our manuscript.

References

Alaska Earthquake Center, Univ. of Alaska Fairbanks. (1987). Alaska Regional Network. International Federation of Digital Seismograph Networks. https://doi.org/10.7914/SN/AK

Alaska Volcano Observatory/USGS. (1988). Alaska Volcano Observatory. International Federation of Digital Seismograph Networks. https://doi.org/10.7914/SN/AV

Albuquerque Seismological Laboratory (ASL)/USGS. (1980). *US Geological Survey Networks*. International Federation of Digital Seismograph Networks. https://doi.org/10.7914/SN/GS

Albuquerque Seismological Laboratory (ASL)/USGS. (1988). Global Seismograph Network - IRIS/USGS. International Federation of Digital Seismograph Networks. https://doi.org/10.7914/SN/IU

Albuquerque Seismological Laboratory (ASL)/USGS. (1990). United States National Seismic Network. International Federation of Digital Seismograph Networks. https://doi.org/10.7914/SN/US

ZHENG ET AL. 9 of 13

- Albuquerque Seismological Laboratory (ASL)/USGS. (1992). New China Digital Seismograph Network. International Federation of Digital Seismograph Networks. https://doi.org/10.7914/SN/IC
- Albuquerque Seismological Laboratory (ASL)/USGS. (1993). Global Telemetered Seismograph Network (USAF/USGS). International Federation of Digital Seismograph Networks. https://doi.org/10.7914/SN/GT
- Albuquerque Seismological Laboratory (ASL)/USGS. (2003). Intermountain West Seismic Network. International Federation of Digital Seismograph Networks, https://doi.org/10.7914/SN/IW
- Albuquerque Seismological Laboratory (ASL)/USGS. (2006). Caribbean USGS Network. International Federation of Digital Seismograph Networks. https://doi.org/10.7914/SN/CU
- Albuquerque Seismological Laboratory (ASL)/USGS. (2013). Central and Eastern US Network. International Federation of Digital Seismograph Networks. https://doi.org/10.7914/SN/N4
- Amores, A., Monserrat, S., Marcos, M., Argüeso, D., Villalonga, J., Jordà, G., & Gomis, D. (2022). Numerical simulation of atmospheric lamb waves generated by the 2022 Hunga-Tonga volcanic eruption. *Geophysical Research Letters*, 49(6), e2022GL098240. https://doi. org/10.1029/2022gl098240
- Behnke, S. A., Thomas, R. J., McNutt, S. R., Schneider, D. J., Krehbiel, P. R., Rison, W., & Edens, H. E. (2013). Observations of volcanic light-ning during the 2009 eruption of Redoubt Volcano. *Journal of Volcanology and Geothermal Research*, 259, 214–234. https://doi.org/10.1016/j.jvolgeores.2011.12.010
- Borrero, J. C., Cronin, S. J., & Latu'ila, F. H. (2022). Tsunami runup and inundation in Tonga from the January 2022 eruption of Hunga volcano, 13 September 2022. PREPRINT (Version 1). Available at Research Square. https://doi.org/10.21203/rs.3.rs-2044907/v1
- Brenna, M., Cronin, S. J., Smith, I. E. M., Pontesilli, A., Tost, M., Barker, S., et al. (2022). Post-caldera volcanism reveals shallow priming of an intra-ocean arc andesitic caldera: Hunga volcano, Tonga, SW Pacific. *Lithos*, 412–413, 106614. https://doi.org/10.1016/j.lithos.2022.106614
- Bureau of Economic Geology, & The University of Texas at Austin. (2016). *Texas Seismological Network*. International Federation of Digital Seismograph Networks. https://doi.org/10.7914/SN/TX
- California Institute of Technology, & United States Geological Survey Pasadena. (1926). Southern California Seismic Network. International Federation of Digital Seismograph Networks. https://doi.org/10.7914/SN/CI
- Carey, S., & Bursik, M. (2015). Chapter 32 Volcanic plumes. In H. Sigurdsson (Ed.), *The encyclopedia of volcanoes* (2nd ed., pp. 571–585). Academic Press, Vol. Series editor.
- Carvajal, M., Sepúlveda, I., Gubler, A., & Garreaud, R. (2022). Worldwide signature of the 2022 Tonga volcanic tsunami. Geophysical Research Letters, n/a(n/a), e2022GL098153. https://doi.org/10.1029/2022gl098153
- Cascades Volcano Observatory/USGS. (2001). Cascade Chain Volcano Monitoring. International Federation of Digital Seismograph Networks.
- https://doi.org/10.7914/SN/CC
 Charles University in Prague (Czech), Institute of Geonics, Institute of Geophysics, Academy of Sciences of the Czech Republic, Institute of Physics of the Earth Masaryk University (Czech), & Institute of Rock Structure and Mechanics. (1973). Czech Regional Seismic Network.
- International Federation of Digital Seismograph Networks. https://doi.org/10.7914/SN/CZ

 Chouet, B., Dawson, P., Ohminato, T., Martini, M., Saccorotti, G., Giudicepietro, F., et al. (2003). Source mechanisms of explosions at Stromboli Volcano, Italy, determined from moment-tensor inversions of very-long-period data. *Journal of Geophysical Research*, 108(B1), ESE7-1–ESE7-25. https://doi.org/10.1029/2002jb001919
- Chouet, B. A., & Matoza, R. S. (2013). A multi-decadal view of seismic methods for detecting precursors of magma movement and eruption. Journal of Volcanology and Geothermal Research, 252, 108–175. https://doi.org/10.1016/j.jvolgeores.2012.11.013
- Colorado Geological Survey. (2016). Colorado Geological Survey Seismic Network. International Federation of Digital Seismograph Networks. https://doi.org/10.7914/SN/C0
- Coppess, K. R., Dunham, E. M., & Almquist, M. (2022). Ultra and very long period seismic signatures of unsteady eruptions predicted from conduit flow models. *Journal of Geophysical Research: Solid Earth*, 127(6), e2022JB024313. https://doi.org/10.1029/2022jb024313
- Cronin, S. J., Brenna, M., Smith, I. E. M., Barker, S. J., Tost, M., Ford, M., et al. (2017). New volcanic island unveils explosive past. *Eos*, 98. Published on 26 June 2017. https://doi.org/10.1029/2017EO076589
- Cronin, S. J., & Tonga Geological Services. (2022). New bathymetry map of Hunga Tonga-Hunga Ha'apai volcano's caldera. Retrieved from https://www.volcanodiscovery.com/hunga-tonga-hunga-haapai/news/181524/Hunga-Tonga-Hunga-Ha-apai-volcano-Tonga-new-bathymetry-map-of-caldera.html
- Dublin Institute for Advanced Studies. (1993). Irish National Seismic Network. International Federation of Digital Seismograph Networks. https://doi.org/10.7914/SN/EI
- Dziewonski, A. M., & Anderson, D. L. (1981). Preliminary reference Earth model. *Physics of the Earth and Planetary Interiors*, 25(4), 297–356. https://doi.org/10.1016/0031-9201(81)90046-7
- Federal Institute for Geosciences and Natural Resources. (1976). German Regional Seismic Network (GRSN). Bundesanstalt für Geowissenschaften und Rohstoffe. https://doi.org/10.25928/mbx6-hr74
- Fowler, S. J., & Spera, F. J. (2008). Phase equilibria trigger for explosive volcanic eruptions. Geophysical Research Letters, 35(8), L08309. https://doi.org/10.1029/2008gl033665
- Garza-Girón, R., Lay, T., Pollitz, F., Kanamori, H., & Rivera, L. (2022). Solid Earth–atmosphere interaction forces during the 15 January 2022 Tonga eruption. Science Advances, 9(2), eadd4931.
- GEOFON Data Centre. (1993). GEOFON Seismic Network. Deutsches GeoForschungsZentrum GFZ. https://doi.org/10.14470/TR560404
- Glanville, H. (2019). Beetaloo seismic monitoring project. International Federation of Digital Seismograph Networks. https://doi.org/10.7914/SN/2O_2019
- Global Volcanism Program. (1988). Report on Hunga Tonga-Hunga Ha'apai (Tonga). In L. McClelland (Ed.), Scientific event alert network bulletin, 13:5. Smithsonian Institution. https://doi.org/10.5479/si.GVP.SEAN198805-243040
- Global Volcanism Program. (2004). Report on Asamayama (Japan). In R. Wunderman (Ed.), Bulletin of the global volcanism network, 29:8.
 Smithsonian Institution. https://doi.org/10.5479/si.GVP.BGVN200408-283110
- Global Volcanism Program. (2009a). Report on Hunga Tonga-Hunga Ha'apai (Tonga). In S. K. Sennert (Ed.), Weekly volcanic activity report, 11 March–17 March 2009. Smithsonian Institution and US Geological Survey. https://doi.org/10.5479/si.GVP.WVAR20090311-243040
- Global Volcanism Program. (2009b). Report on Hunga Tonga-Hunga Ha'apai (Tonga). In S. K. Sennert (Ed.), Weekly volcanic activity report, 18 March-24 March 2009. Smithsonian Institution and US Geological Survey. https://doi.org/10.5479/si.GVP.WVAR20090318-243040
- Global Volcanism Program. (2015). Report on Hunga Tonga-Hunga Ha'apai (Tonga). In R. Wunderman (Ed.), Bulletin of the global volcanism network 40(1). Smithsonian Institution. https://doi.org/10.5479/si.GVP.BGVN201501-243040
- Global Volcanism Program. (2022a). Report on Hunga Tonga-Hunga Ha'apai (Tonga). In K. L. Bennis & E. Venzke (Eds.), Bulletin of the global volcanism network 47(3). Smithsonian Institution. https://doi.org/10.5479/si.GVP.BGVN202203-243040

ZHENG ET AL. 10 of 13

- Global Volcanism Program. (2022b). Report on Hunga Tonga-Hunga Ha'apai (Tonga). In S. K. Sennert (Ed.), Weekly volcanic activity report, 12 January–18 January 2022. Smithsonian Institution and U.S. Geological Survey.
- GNS Science. (2021). GeoNet Aotearoa New Zealand Seismic Digital Waveform Dataset. GNS Science. https://doi.org/10.21420/G19Y-9D40 Gualda, G. A. R., & Ghiorso, M. S. (2015). MELTS_Excel: A Microsoft Excel-based MELTS interface for research and teaching of magma properties and evolution. Geochemistry, Geophysics, Geosystems, 16(1), 315–324. https://doi.org/10.1002/2014gc005545
- Hoblitt, R. P. (1994). An experiment to detect and locate lightning associated with eruptions of redoubt volcano. *Journal of Volcanology and Geothermal Research*, 62(1–4), 499–517. https://doi.org/10.1016/0377-0273(94)90049-3
- Imamura, F., Suppasri, A., Arikawa, T., Koshimura, S., Satake, K., & Tanioka, Y. (2022). Preliminary observations and impact in Japan of the Tsunami caused by the Tonga volcanic eruption on January 15, 2022. Pure and Applied Geophysics, 179(5), 1549–1560. https://doi. org/10.1007/s00024-022-03058-0
- Incorporated Research Institutions For Seismology. (1970). SINGLE STATION. International Federation of Digital Seismograph Networks. https://doi.org/10.7914/SN/SS
- INGEOMINAS Servicio Geologico Colombiano (SGC Colombia). (1993). Red Sismologica Nacional de Colombia. International Federation of Digital Seismograph Networks. https://doi.org/10.7914/SN/CM
- Institut de physique du globe de Paris (IPGP), & École et Observatoire des Sciences de la Terre de Strasbourg (EOST). (1982). GEOSCOPE, French Global Network of broad band seismic stations. Institut de physique du globe de Paris (IPGP), Université de Paris. https://doi.org/10.18715/GEOSCOPE.G
- Instituto Dom Luiz (IDL) Faculdade de Ciências da Universidade de Lisboa. (2003). University of Lisbon Seismic Network. International Federation of Digital Seismograph Networks. https://doi.org/10.7914/SN/LX
- Instituto Nicaraguense de Estudios Territoriales (INETER). (1975). Nicaraguan Seismic Network. International Federation of Digital Seismograph Networks. https://doi.org/10.7914/SN/NU
- Instituto Português do Mar e da Atmosfera, I.P. (2006). Portuguese National Seismic Network. International Federation of Digital Seismograph Networks. https://doi.org/10.7914/SN/PM
- IRIS Transportable Array. (2003). USArray Transportable Array. International Federation of Digital Seismograph Networks. https://doi.org/10.7914/SN/TA
- Iverson, R. M., Dzurisin, D., Gardner, C. A., Gerlach, T. M., LaHusen, R. G., Lisowski, M., et al. (2006). Dynamics of seismogenic volcanic extrusion at Mount St Helens in 2004–05. *Nature*, 444(7118), 439–443. https://doi.org/10.1038/nature05322
- extrusion at Mount St Helens in 2004–05. *Nature*, 444(/118), 439–443. https://doi.org/10.1038/nature05322

 Kanamori, H., & Given, J. W. (1982). Analysis of long-period seismic-waves excited by the May 18, 1980, eruption of Mount St Helens A
- terrestrial monopole. *Journal of Geophysical Research*, 87(NB7), 5422–5432. https://doi.org/10.1029/jb087ib07p05422 Kieffer, S. W. (1984). Seismicity at old faithful geyser - An isolated source of geothermal noise and possible analog of volcanic seismicity. *Jour-*
- nal of Volcanology and Geothermal Research, 22(1–2), 59–95. https://doi.org/10.1016/0377-0273(84)90035-0

 Kintner, J. A., Yeck, W. L., Earle, P. S., Prejean, S., & Pesicek, J. D. (2022). High-precision characterization of seismicity from the 2022 Hunga
- Tonga-Hunga Ha'apai volcanic eruption. Seismological Research Letters, 94(2A), 589–602. https://doi.org/10.1785/0220220250
- KNMI. (1993). Netherlands Seismic and Acoustic Network. Royal Netherlands Meteorological Institute (KNMI). https://doi.org/10.21944/e970fd34-23b9-3411-b366-e4f72877d2c5
- KNMI. (2006). Caribbean Netherlands Seismic Network. Royal Netherlands Meteorological Institute (KNMI). https://doi.org/10.21944/dffa7a3f-7e3a-3b33-a436-516a01b6af3f
- Knopoff, L., & Randall, M. J. (1970). Compensated linear-vector dipole A possible mechanism for deep earthquakes. *Journal of Geophysical Research*, 75(26), 4957–4963. https://doi.org/10.1029/jb075i026p04957
- Kubota, T., Saito, T., & Nishida, K. (2022). Global fast-traveling tsunamis driven by atmospheric Lamb waves on the 2022 Tonga eruption. Science, 377(6601), 91–94. https://doi.org/10.1126/science.abo4364
- Lamont Doherty Earth Observatory (LDEO), Columbia University. (1970). Lamont-Doherty Cooperative Seismographic Network. International Federation of Digital Seismograph Networks. https://doi.org/10.7914/SN/LD
- Lister, J. R., & Kerr, R. C. (1991). Fluid-mechanical models of crack propagation and their application to magma transport in dykes. *Journal of Geophysical Research*, 96(B6), 10049–10077. https://doi.org/10.1029/91jb00600
- Matoza, R. S., Fee, D., Assink, J. D., Iezzi, A. M., Green, D. N., Kim, K., et al. (2022). Atmospheric waves and global seismoacoustic observations of the January 2022 Hunga eruption, Tonga. *Science*, 377(6601), 95–100. https://doi.org/10.1126/science.abo7063
- MedNet Project Partner Institutions. (1990). Mediterranean Very Broadband Seismographic Network (MedNet). Istituto Nazionale di Geofisica e Vulcanologia (INGV). https://doi.org/10.13127/SD/fBBBtDtd6q
- Morrissey, M. M., & Chouet, B. A. (1997). A numerical investigation of choked flow dynamics and its application to the triggering mechanism of long-period events at Redoubt Volcano, Alaska, *Journal of Geophysical Research*, 102(B4), 7965–7983, https://doi.org/10.1029/97ib00023
- Multiple Operators. (1997). International Geodynamics and Earth Tide Service. International Federation of Digital Seismograph Networks. https://doi.org/10.7914/SN/SG
- National Institute for Earth Physics (NIEP Romania). (1994). Romanian Seismic Network. International Federation of Digital Seismograph Networks. https://doi.org/10.7914/SN/RO
- Natural Resources Canada (NRCAN Canada). (1975). Canadian National Seismograph Network. International Federation of Digital Seismograph Networks. https://doi.org/10.7914/SN/CN
- NOAA National Oceanic and Atmospheric Administration (USA). (1967). National Tsunami Warning Center Alaska Seismic Network. International Federation of Digital Seismograph Networks. https://doi.org/10.7914/SN/AT
- Northern California Earthquake Data Center. (2014). Berkeley Digital Seismic Network (BDSN). Northern California Earthquake Data Center. https://doi.org/10.7932/BDSN
- Ohminato, T., Takeo, M., Kumagai, H., Yamashina, T., Oikawa, J., Koyama, E., et al. (2006). Vulcanian eruptions with dominant single force components observed during the Asama 2004 volcanic activity in Japan. *Earth Planets and Space*, 58(5), 583–593. https://doi.org/10.1186/
- Poli, P., & Shapiro, N. M. (2022). Rapid characterization of large volcanic eruptions: Measuring the impulse of the Hunga Tonga Ha'apai explosion from teleseismic waves. *Geophysical Research Letters*, 49(8), e2022GL098123. https://doi.org/10.1029/2022gl098123
- Red Sísmica Mexicana. (n.d.). https://doi.org/10.21766/SSNMX/SN/MX
- San Fernando Royal Naval Observatory (ROA), Universidad Complutense De Madrid (UCM), Helmholtz-Zentrum Potsdam Deutsches GeoForschungsZentrum (GFZ), Universidade De Evora (UEVORA, Portugal), & Institute Scientifique Of RABAT (ISRABAT, Morocco). (1996). The Western Mediterranean BB seismic Network. Deutsches GeoForschungsZentrum GFZ. https://doi.org/10.14470/IZ581150
- Scripps Institution of Oceanography. (1986). Global Seismograph Network IRIS/IDA. International Federation of Digital Seismograph Networks. https://doi.org/10.7914/SN/II

ZHENG ET AL. 11 of 13



Geophysical Research Letters

- 10.1029/2023GL102763
- Smith, I. E. M., & Price, R. C. (2006). Tonga-Kermadec arc and Havre-Lau back-arc system: Their role in the development of tectonic and magmatic models for the western Pacific. *Journal of Volcanology and Geothermal Research*, 156(3–4), 315–331. https://doi.org/10.1016/j.ivolgeores.2006.03.006
- St. Lawrence, W., & Qamar, A. (1979). Hydraulic transients: A seismic source in volcanoes and glaciers. Science, 203(4381), 654–656. https://doi.org/10.1126/science.203.4381.654
- Streeter, V. L., & Wylie, E. B. (1974). Waterhammer and surge control. Annual Review of Fluid Mechanics, 6(1), 57–73. https://doi.org/10.1146/annurev.fl.06.010174.000421
- Swiss Seismological Service (SED) At ETH Zurich. (1983). National Seismic Networks of Switzerland. ETH Zürich. https://doi.org/10.12686/sed/networks/ch
- Tait, S., Jaupart, C., & Vergniolle, S. (1989). Pressure, gas content and eruption periodicity of a shallow, crystallizing magma chamber. *Earth and Planetary Science Letters*, 92(1), 107–123. https://doi.org/10.1016/0012-821x(89)90025-3
- Terry, J. P., Goff, J., Winspear, N., Bongolan, V. P., & Fisher, S. (2022). Tonga volcanic eruption and tsunami, January 2022: Globally the most significant opportunity to observe an explosive and tsunamigenic submarine eruption since AD 1883 Krakatau. *Geoscience Letters*, 9(1), 24. https://doi.org/10.1186/s40562-022-00232-z
- Thurin, J., Tape, C., & Modrak, R. (2022). Multi-event explosive seismic source for the 2022 Mw 6.3 Hunga Tonga submarine volcanic eruption. The Seismic Record, 2(4), 217–226. https://doi.org/10.1785/0320220027
- UC San Diego. (1982). ANZA Regional Network. International Federation of Digital Seismograph Networks. https://doi.org/10.7914/SN/AZ
- UC San Diego. (2014). Piñon Flats Observatory Array. International Federation of Digital Seismograph Networks. https://doi.org/10.7914/SN/PY
- UC Santa Barbara. (1989). UC Santa Barbara Engineering Seismology Network. International Federation of Digital Seismograph Networks. https://doi.org/10.7914/SN/SB
- Universidad de Chile. (2012). Red Sismologica Nacional. International Federation of Digital Seismograph Networks. https://doi.org/10.7914/ SN/C1
- University of Oregon. (1990). Pacific Northwest Seismic Network University of Oregon. International Federation of Digital Seismograph Networks. https://doi.org/10.7914/SN/UO
- University of Utah. (1962). University of Utah Regional Seismic Network. International Federation of Digital Seismograph Networks. https://doi.org/10.7914/SN/UU
- University of Utah. (1983). Yellowstone National Park Seismograph Network. International Federation of Digital Seismograph Networks. https://doi.org/10.7914/SN/WY
- USGS. (2022). M5.8 volcanic eruption 68 km NNW of Nuku'alofa, Tonga. Retrieved from https://earthquake.usgs.gov/earthquakes/eventpage/us7000cc8r/executive
- us7000gc8r/executive
 USGS Hawaiian Volcano Observatory (HVO). (1956). Hawaiian Volcano Observatory Network. International Federation of Digital Seismograph
- Networks. https://doi.org/10.7914/SN/HV
 Vergoz, J., Hupe, P., Listowski, C., Le Pichon, A., Garcés, M. A., Marchetti, E., et al. (2022). IMS observations of infrasound and acoustic-gravity waves produced by the January 2022 volcanic eruption of Hunga, Tonga: A global analysis. *Earth and Planetary Science Letters*, 591, 117639. https://doi.org/10.1016/j.eps1.2022.117639
- Wei, S. S., Zha, Y., Shen, W., Wiens, D. A., Conder, J. A., & Webb, S. C. (2016). Upper mantle structure of the Tonga-Lau-Fiji region from Rayleigh wave tomography. *Geochemistry, Geophysics, Geosystems*, 17(11), 4705–4724. https://doi.org/10.1002/2016gc006656
- Wright, C. J., Hindley, N. P., Alexander, M. J., Barlow, M., Hoffmann, L., Mitchell, C. N., et al. (2022). Surface-to-space atmospheric waves from Hunga Tonga-Hunga Ha'apai eruption. *Nature*, 609(7928), 741–746. https://doi.org/10.1038/s41586-022-05012-5
- Xu, J., Li, D., Bai, Z., Tao, M., & Bian, J. (2022). Large amounts of water vapor were injected into the stratosphere by the Hunga Tonga–Hunga Ha'apai volcano eruption. *Atmosphere*, 13(6), 912.
- Yin, A. (2018). Water hammers tremors during plate convergence. *Geology*, 46(12), 1031–1034. https://doi.org/10.1130/g45261.1
- Yu, C., Zheng, Y., & Shang, X. (2017). Crazyseismic: A MATLAB GUI-based software package for passive seismic data preprocessing. Seismological Research Letters, 88(2A), 410–415. https://doi.org/10.1785/0220160207
- Yuen, D. A., Scruggs, M. A., Spera, F. J., Zheng, Y., Hu, H., McNutt, S. R., et al. (2022). Under the surface: Pressure-induced planetary-scale waves, volcanic lightning, and gaseous clouds caused by the submarine eruption of Hunga Tonga-Hunga Ha'apai volcano. *Earthquake Research Advances*, 2(3), 100134. https://doi.org/10.1016/j.eqrea.2022.100134
- ZAMG Zentralanstalt für Meterologie und Geodynamik. (1987). Austrian Seismic Network. International Federation of Digital Seismograph Networks. https://doi.org/10.7914/SN/OE

References From the Supporting Information

encyclopedia of volcanoes (2nd ed, pp. 459-471).

- Baag, C. E., & Langston, C. A. (1985). Shear-coupled PL. Geophysical Journal International, 80(2), 363–385. https://doi.org/10.1111/j.1365-246x.1985.tb05100.x
- Barmin, A. A., & Melnik, O. E. (1996). Modelling of nonstationary processes of high-viscous gas saturated volcanic eruption magma. *Vestnik MGU Seriya 1. Matematika and Mekhanika*, 4, 91–98. [In Russian].
- Buresti, G., & Casarosa, C. (1989). One-dimensional adiabatic flow of equilibrium gas-particle mixtures in long vertical ducts with friction. Journal of Fluid Mechanics, 203, 251–272. https://doi.org/10.1017/s002211208900145x
- Cas, R. A. F., & Simmons, J. M. (2018). Why deep-water eruptions are so different from subaerial eruptions. Frontiers of Earth Science, 6, 198.
- https://doi.org/10.3389/feart.2018.00198

 Cashman, K. V., & Scheu, B. (2015). Magmatic fragmentation. In H. Sigurdsson, B. Houghton, S. McNutt, H. Rymer, & J. Stix (Eds.), *The*
- Chojnicki, K., Clarke, A. B., & Phillips, J. C. (2006). A shock-tube investigation of the dynamics of gas-particle mixtures: Implications for explosive volcanic eruptions. Geophysical Research Letters, 33(15), L15309. https://doi.org/10.1029/2006GL026414
- Cooker, M. J., & Peregrine, D. H. (1995). Pressure-impulse theory for liquid impact problems. *Journal of Fluid Mechanics*, 297, 193–214. https://doi.org/10.1017/s0022112095003053
- Gonnerman, H. M., & Manga, M. (2013). Dynamics of magma ascent in the volcanic conduit. In S. A. Fagents, T. K. P. Gregg, & R. M. C. Lopez (Eds.), *Modeling volcanic processes*. Cambridge University Press.
- Haar, L., Gallagher, J. S., & Kell, G. S. (1984). NBS/NRC steam tables thermodynamic and transport properties and computer programs for vapor and liquid states of water in SI units. Hemisphere Pub. Corp.

ZHENG ET AL. 12 of 13

- Henry, R. E., & Fauske, H. K. (1968). Propagation velocity of pressure waves in two-phase mixtures and the dependency on flow regimes. *Transactions of the American Nuclear Society*, 11, 364–365.
- Joukowsky, N. (1898). On the hydraulic hammer in water supply pipes. Mémoires de l'Académie Impériale des Sciences de St.-Pétersbourg (1900), Series 8, 9(5), 1–71. [In German].
- Kleinstreuer, C. (2003). Two-phase flow: Theory and applications (1st ed.). Taylor & Francis.
- Kieffer, S. W., & Sturtevant, B. (1984). Laboratory studies of volcanic jets. Journal of Geophysical Research, 89(B10), 8253–8268. https://doi.org/10.1029/jb089jb10p08253
- Kiyama, A., Tagawa, Y., Ando, K., & Kameda, M. (2016). Effects of a water hammer and cavitation on jet formation in a test tube. *Journal of Fluid Mechanics*, 787, 224–236. https://doi.org/10.1017/jfm.2015.690
- La Spina, G., Arzilli, F., Burton, M. R., Polacci, M., & Clarke, A. B. (2022). Role of volatiles in highly explosive basaltic eruptions. *Nature Communications Earth & Environment*, 3(1), 156. https://doi.org/10.1038/s43247-022-00479-6
- La Spina, G., Clarke, A. B., de'Michieli Vitturi, M., Burton, M., Allison, C. M., Roggensack, K., & Alfano, F. (2019). Conduit dynamics of highly explosive basaltic eruptions: The 1085 CE Sunset Crater sub-plinian events. *Journal of Volcanology and Geothermal Research*, 387, 106658. https://doi.org/10.1016/j.jvolgeores.2019.08.001
- Lesher, C. E., & Spera, F. J. (2015). Thermodynamic and transport properties of silicate melts and magma. In H. Sigurdsson, B. Houghton, H. Rymer, J. Stix, & S. McNutt (Eds.), *The encyclopedia of volcanoes* (pp. 113–141). Vol. Series editor.
- Livshits, L. D., & Bolkhovitinov, L. G. (1977). Weak shock waves in the eruption column. Nature, 267(5610), 420–421. https://doi. org/10.1038/267420a0
- Macedonio, G., Dobran, F., & Neri, A. (1994). Erosion processes in volcanic conduits and application to the AD 79 eruption of Vesuvius. Earth and Planetary Science Letters, 121(1-2), 137-152. https://doi.org/10.1016/0012-821x(94)90037-x
- McBirney, A. R. (1973). Factors governing the intensity of explosive andesitic eruptions. Bulletin Volcanologique, 37(3), 443–453. https://doi.org/10.1007/bf02597641
- McNutt, S. R., & Thomas, R. J. (2015). Volcanic lightning. In H. Sigurdsson, B. Houghton, S. McNutt, H. Rymer, & J. Stix (Eds.), *The encyclopedia of volcanoes* (2nd ed. pp. 1061–1067).
- Melnik, O. (2000). Dynamics of two-phase conduit flow of high-viscosity gas-saturated magma: Large variations of sustained explosive eruption intensity. *Bulletin of Volcanology*, 62(3), 153–170. https://doi.org/10.1007/s004450000072
- Newcombe, M. E., Plank, T., Zhang, Y., Holycross, M., Barth, A., Lloyd, A. S., et al. (2020). Magma pressure-temperature-time paths during mafic explosive eruptions. Frontiers of Earth Science, 8, 531911. https://doi.org/10.3389/feart.2020.531911
- Nissen-Meyer, T., van Driel, M., Stähler, S. C., Hosseini, K., Hempel, S., Auer, L., et al. (2014). AxiSEM: Broadband 3-D seismic wavefields in axisymmetric media. *Solid Earth*, 5(1), 425–445. https://doi.org/10.5194/se-5-425-2014
- Schreier, S. (1982). Compressible flow. John Wiley and Sons.
- Slezin, Y. B. (1991). Variation of the mass flow rates during a large explosive eruption. Vulkanologiya i Seismologiya, 1, 35-43.
- Sparks, R. S. J., & Bursik, M. I. (1997). Volcanic plumes. John Wiley and Sons.
- Wallis, G. B. (1969). One-dimensional two-phase flow. McGraw-Hill.
- Woods, A. W., & Bower, S. M. (1995). The decompression of volcanic jets in a crater during explosive volcanic eruptions. *Earth and Planetary Science Letters*, 131(3-4), 189–205. https://doi.org/10.1016/0012-821x(95)00012-2
- Zheng, Y., Hu, H., Spera, F. J., Scruggs, M., Thompson, G., Jin, Y., et al. (2023). Dataset: Episodic magma hammers for the 15 January 2022 cataclysmic eruption of Hunga Tonga-Hunga Ha'apai. Edited, Texas Data Repository. https://doi.org/10.18738/T8/W6JN20

ZHENG ET AL. 13 of 13